ACS Photonics

Article

Cite This: ACS Photonics 2018, 5, 4896−4902

pubs.acs.org/journal/apchd5

InGaAs-Based Well−Island Composite Quantum-Confined Structure with Superwide and Uniform Gain Distribution for Great Enhancement of Semiconductor Laser Performance

Qingnan Yu,[†] Xue Li,[‡] Yan Jia,[†] Wei Lu,[†] Ming Zheng,[†] Xing Zhang,[‡] Yongqiang Ning,[‡] and Jian Wu*[,†]

[†]Department of Applied Physics, Beihang University, Beijing 100191, China

[‡]State Key Laboratory of Luminescence and Application, Changchun Institute of Optics, Fine Mechanics and Physics, Chinese Academy of Sciences, Changchun 130033, China

Downloaded via CHINESE ACADEMY OF SCIENCES on May 20, 2019 at 06:30:13 (UTC).
See https://pubs.acs.org/sharingguidelines for options on how to legitimately share published articles.

ABSTRACT: In the development of semiconductor lasers, it has been a dream all along to simultaneously obtain extremely wide and uniform gain distribution, because such a gain configuration can greatly enhance semiconductor laser performance. Hence, it has also been a huge challenge to realize this dream so far. In this paper, we are reporting a special InGaAs-based well−island composite quantum-confined structure, with which the best results to date in achieving both superwide and very uniform gain and power distributions are obtained. The spectral flatness of the output power can reach 0.1 dB, and the gain bandwidth is broadened to 6-fold broader than the fwhm (full width at half-maximum) of the standard gain spectrum from a classic InGaAs quantum well under the same carrier density. The formation of the well−island composite quantum-confined structure is associated with the indium-rich island effect in the material growth. The great significance of this work lies in that it is making the above dream come true, since it not only can tremendously increase the spectral tuning range of an InGaAs-based semiconductor laser but also exhibits a great potential on achieving uniform output power over the full spectral tuning range of the laser.

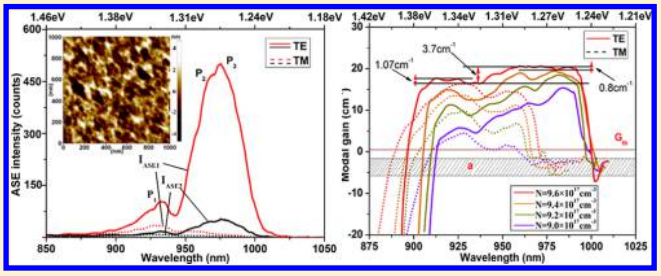

KEYWORDS: *tunable semiconductor lasers, well−island composite quantum-confined structure, InGaAs/GaAs material, gain characteristics, flat top, indium-rich islands*

It has been well known that semiconductor lasers are taking important roles in many application fields.[1−4] However, the current quantum confined structures provide semiconductor lasers with a very limited bandwidth and nonuniform distribution of gains, such as the typical gain spectrum of a single InGaAs/GaAs quantum well, which is described in Figure 1a. This leads to a narrow spectral tuning range and nonuniform output power on all cavity modes due to the nature of the structure so that the further enhancement of semiconductor laser performance is restricted. Tunable diode lasers are a typical example, in which lasing power is apparently reduced at both ends of the spectral tuning range, apart from the finite wavelength tuning range. This is illustrated in Figure 1b. This problem actually exists in other types of tunable lasers as well, which is shown in Figure 1c. Hence, the great enhancement of both spectral tuning range and uniformity of the lasing power is always expected for the tunable lasers. For this reason, scientists have been seeking out new techniques to obtain a more uniform (flat-top) gain distribution with a broader bandwidth for tunable semiconductor lasers.[5−21] This work is still in progress, and no effective approach or new quantum-confined structure has been found to significantly change the current situation so far. In all existing techniques, only a few approaches have shown a certain improvement on both gain uniformity (flatness) and bandwidth.

In order to evaluate the capacity of the quantum-confined structure for achieving and broadening the flat top of the gain or power spectrum, a flat-top broadening factor, RSW, is defined as a measure of the broadening degree here. It is a ratio of the flat-top width of the broadened gain or power spectrum to the bandwidth (fwhm) of the standard gain or power spectrum from a typical single quantum-confined structure based on the same materials and similar operation conditions. One common approach for improvement of both uniformity and bandwidth of the gain or power spectrum is the longitudinal combination of multiple quantum wells or quantum dot layers along the growth direction. These wells or dot layers have different band gaps to produce mutually offset gain or power spectra and their superposition.[17−21] This approach can properly increase the bandwidth and uniformity of the total gain or power spectrum due to the superposition effect. For example, the RSW reached 3.8 with the flatness of ∼3 dB for an ASE spectrum of the InAs quantum dot

Received: July 29, 2018
Published: November 1, 2018

© 2018 American Chemical Society

DOI: 10.1021/acsphotonics.8b01048
ACS Photonics 2018, 5, 4896−4902

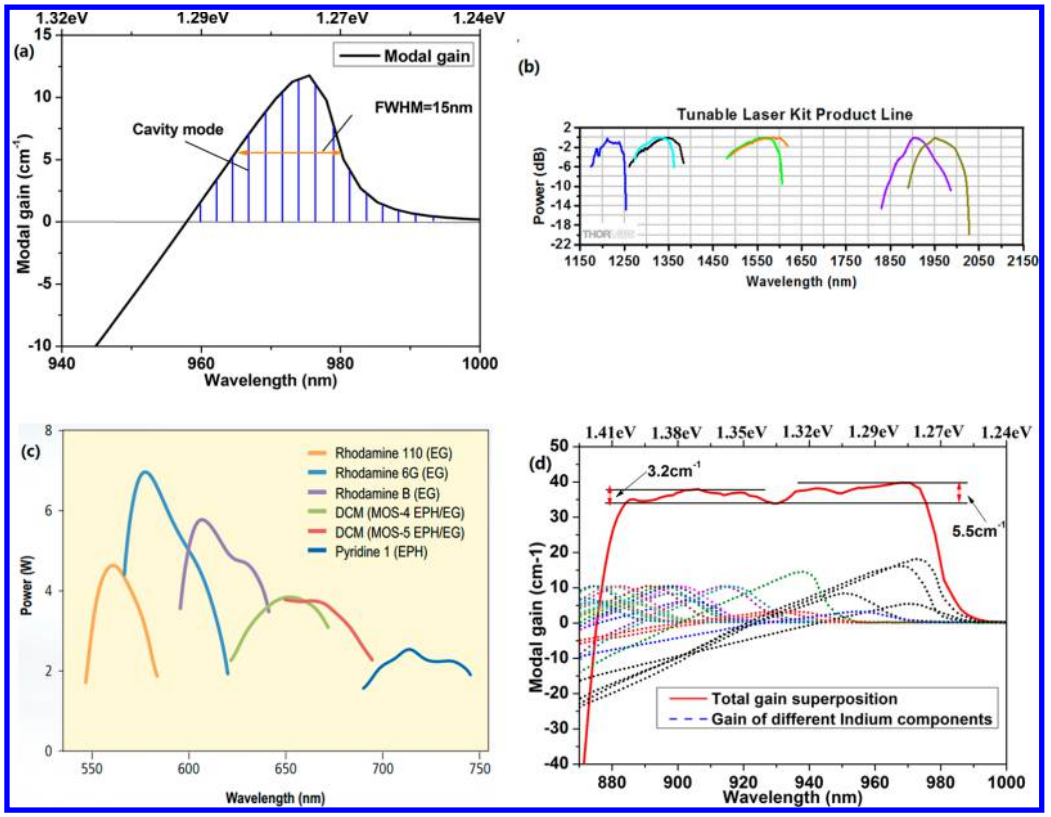

Figure 1. (a) Calculated modal gain of a single InGaAs/GaAs/GaAsP quantum well and cavity modes with the experimental carrier density of 9.6 × 10^{17}cm^{-3}. (b and c) Data of powers as functions of wavelengths from tunable diode laser products (Thorlabs, model TLK-L) and tunable dye laser products (Spectra-physics, model Matisse 2), respectively. (d) Simulation of the gain superposition from 20 InGaAs/GaAs/GaAsP wells with different indium contents or well widths.

structure,[20] and the RSW was about 2.5 with a flatness of ∼1.2 dB for the ASE spectrum of the InGaAsP/InP multiple-quantum-well structure[19] to date, where ASE denotes the amplified spontaneous emission and flatness denotes the ripple of the flat top of the gain or power spectrum. These results show that the simultaneous improvement on both RSW and flatness of the gain or power spectrum is still limited and difficult. The theoretical simulation on the gain superposition of the InGaAs/GaAs/GaAsP multiple quantum wells using PICS3D software computation shows that it is hardly possible to realize both superwide and uniform gain distributions (e.g., RSW ≥ 6.0 and flatness <5.5 cm^{-1}, where the smallest ripple < 3.2 cm^{-1}; the results are described in the second section) using only a few InGaAs quantum wells or quantum dot layers with different offset gains. This is shown in Figure 1d, in which 20 wells with different indium contents or well widths are required to achieve the superwide and uniform gain distribution due to the gain superposition, where different indium contents or well widths result in varied peak gain wavelengths and gain levels between the wells. Each dot curve denotes the gain spectrum from a single well, and the solid curve is the superposition of all dot curves, i.e., the gain superposition. However, the use of too many wells or dot layers will bring other troubles and difficulties in device fabrication and operation.

The other approach is the use of diode arrays, in which diode elements can work at different cavity modes or wavelengths.[14,16] In this approach, the spectral tuning range of the InGaAs array was properly broadened to 35 nm (fwhm), and the cavity modes from different elements can obtain different gains by controlling the injection power to each element to achieve a more uniform gain or power distribution. This approach can be called lateral combination of the multiple quantum wells. It is not suitable for continuous tuning of the wavelengths and leads to noncoaxial lasing beams. The gain bandwidth and uniformity of the array will be dependent on the element numbers.

In this paper, we are reporting a special InGaAs-based well−island composite quantum-confined structure, with which the superwide gain bandwidth or spectral tuning range with RSW ≥ 6 and very uniform spectral power with the flatness of 0.1 dB can be achieved. The text is arranged as follows. The InGaAs-based well−island composite quantum-confined structure is described first. Then, the optical gain characteristics and complex energy bands relating to a mixing strain state generated in the structure are analyzed. Eventually, lasing power variation with wavelengths based on the structure is evaluated and the conclusion is stated.

INGAAS-BASED WELL−ISLAND COMPOSITE QUANTUM-CONFINED STRUCTURE

The theoretical simulation in Figure 1d shows that to obtain both superwide and uniform gain distribution for an InGaAs-based material system, about 20 gain spectra with different offsets and levels may be required for superposition. This means that about 20 quantum wells with different indium contents or widths are required, most of which produce the gain spectra in the shorter wavelength direction. The slight offsets between the gains mean tiny differences of indium contents for different InGaAs quantum wells so that it is very difficult to control tiny differences of the indium contents

DOI: 10.1021/acsphotonics.8b01048
ACS Photonics 2018, 5, 4896−4902

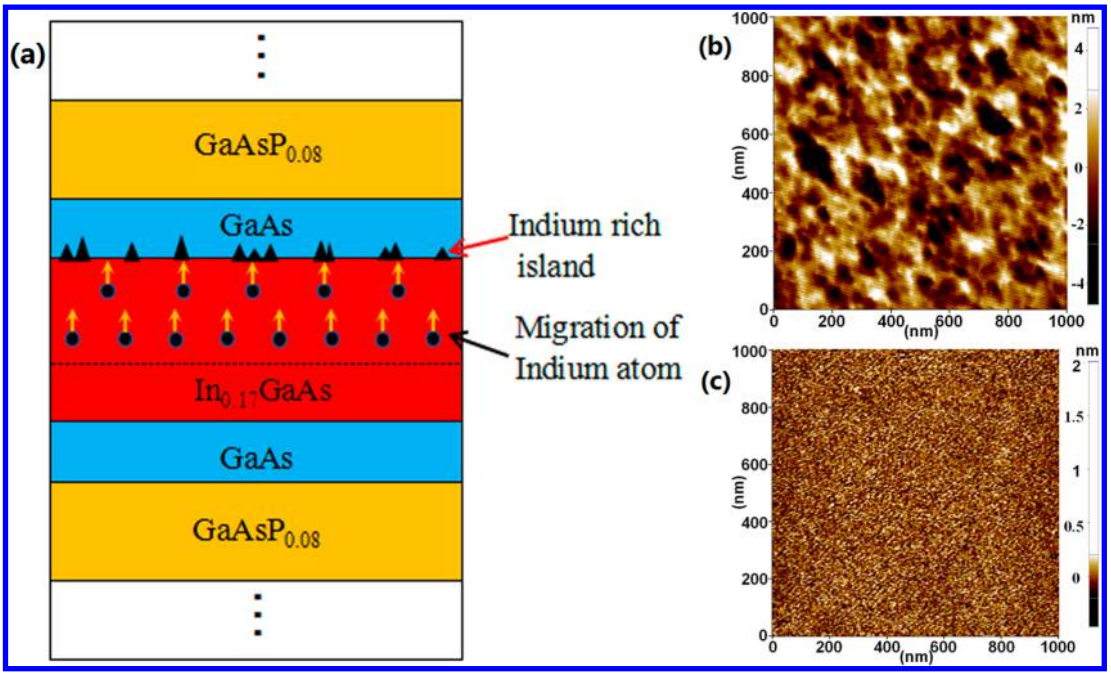

Figure 2. (a) Basic material composition of the InGaAs-based well−island composite quantum-confined structure and the principle of indium-rich island formation. (b) AFM photograph of the exposed InGaAs surface of the $In_{0.17}Ga_{0.83}As/GaAs/GaAsP_{0.08}$ well−island composite structure. (c) AFM photograph of the exposed GaAs surface of an unstrained GaAs/AlGaAs quantum well structure. The samples for (b) and (c) are processed in the same conditions.

between multiple quantum wells in the InGaAs material growth. In fact, the use of too many wells or dot layers will also lead to other troubles in device operation and reliability, etc.

To overcome this difficulty, a special InGaAs-based well−island composite quantum-confined structure is proposed for the first time. This structure is associated with the indium-rich island effect, in which the indium-rich islands were commonly regarded as a sort of defect to avoid for any classic InGaAs quantum well structure so that its special optical characteristics were ignored in the past.[22] The fundamental principle of the indium-rich island formation is that in the growth process of an $In_xGa_{1-x}As/GaAs$ quantum-confined structure, indium atoms would migrate upward to the surface along the material growth direction and form many clusters on the surface of $In_xGa_{1-x}As$ to relax high strain in the $In_xGa_{1-x}As$ layer after the $In_xGa_{1-x}As$ is grown to exceed a few monolayers on the GaAs, as the migration length of the indium atoms is much larger than that of the gallium atoms. This is called the indium-rich island effect. Our investigation shows that the most important factors affecting the island generation are the thickness of $In_xGa_{1-x}As$ layer and the indium content, i.e., x-value in $In_xGa_{1-x}As$, as these two factors dominate the strain accumulation. When the InGaAs layer exceeds a certain thickness and the x-value in $In_xGa_{1-x}As$ is more than a certain value, e.g., $x \geq 0.15$, the In-rich island effect will happen due to the large accumulated strain.[23,24] Sizes and distributions of the indium-rich islands are generally random and associated with material composition, structure, and growth conditions. Since the indium-rich islands reduce the indium contents in the corresponding InGaAs regions, which are close to the surface of the InGaAs layer, many indium-deficient InGaAs regions are generated and distribute in both growth and in-plane directions. This effect is illustrated in Figure 2, in which Figure 2a describes the InGaAs-based well−island composite quantum-confined structure and its formation mechanism, and Figure 2b shows probable indium-rich islands formed on the InGaAs surface of our samples, which are confirmed by a subsequent ASE spectrum analysis. A large amount of indium-rich islands with a random distribution and various sizes in Figure 2b lead to many discrete indium-deficient InGaAs active regions. These discrete indium-deficient InGaAs active regions have different indium contents and areas, which produce emissions with different peak offsets. So it becomes possible to meet the conditions theoretically described in Figure 1d for achieving the superwide and uniform gain distribution.

The basic material composition of the samples was $In_{0.17}Ga_{0.83}As/GaAs/GaAsP_{0.08}$, where $In_{0.17}Ga_{0.83}As$ was 10 nm in thickness to generate enough strain accumulation and the indium-rich island effect. According to the above analysis, the thinner InGaAs layer and a lower x-value in $In_xGa_{1-x}As$ is not enough to obtain the indium-rich islands.[23] GaAs was the 2-nm-thick strain-compensating layer embedded between $In_{0.17}Ga_{0.83}As$ and $GaAsP_{0.08}$ layers. Both $In_{0.17}Ga_{0.83}As$ and GaAs layers were sandwiched by 8-nm-thick $GaAs_{0.92}P_{0.08}$ barriers. The sample was deposited at a rate of 0.75 μm/h and 100 mbar pressure under 660 °C from the metal organic chemical vapor deposition. The high temperature of 660 °C was applied for increasing the migration length of the indium atoms and is beneficial to the formation of indium-rich islands in the material growth. The V/III ratio was 40 for the structure growth. The InGaAs layer was grown on a (001) semi-insulating GaAs substrate.

In order to observe and measure the indium-rich islands formed on the InGaAs surface, the sample was processed to have the InGaAs layer exposed. Then, its appearance was recorded using an atomic force microscope (AFM) (Park Systems Instrument Co., Ltd., model XE100, with a resolution of 4 nm) and shown in Figure 2b. Also, an unstrained GaAs/AlGaAs quantum well sample was processed in the same conditions, and the exposed GaAs surface was observed using

DOI: 10.1021/acsphotonics.8b01048
ACS Photonics 2018, 5, 4896−4902

AFM to initially make sure the clusters appearing on the InGaAs surface were indium-rich islands rather than other defects from the processing by comparing them. The result was shown in Figure 2c. If any other defects are generated on the GaAs surface due to the processing, they should be observed as well, as it is impossible to generate any islands in the unstrained GaAs/AlGaAs well structure. The result showed that no cluster was observed on the GaAs surface. Therefore, we can initially consider that the InGaAs-based well−island composite structure was established in the sample. The indium-rich island formation in the sample is finally confirmed by the ASE spectrum analysis in the next section. From Figure 2b, the island sizes vary 20−200 nm in width and 2−8 nm in height, respectively.

OPTICAL GAIN CHARACTERISTICS OF THE STRUCTURE

In order to look at optical gain characteristics of the InGaAs-based well−island composite structure, the ASE spectra in both transverse electric (TE) and transverse magnetic (TM) polarizations from the structure were measured. The experimental sample was processed into an in-plane configuration of 1.5 mm × 0.5 mm in size. It was coated by the transmittance of T = 99.99% at one end and uncoated at the other end. The sample was optically pumped from the top using a pulsed 808 nm laser beam with the intensity homogenized in the cross-section under room temperature. The ASE spectra from both facets of the in-plane sample were measured. The measurement principle and results are shown in Figure 3, where I_{sp} denotes the spontaneous emission intensity and R is the reflectivity of the facet without coating.

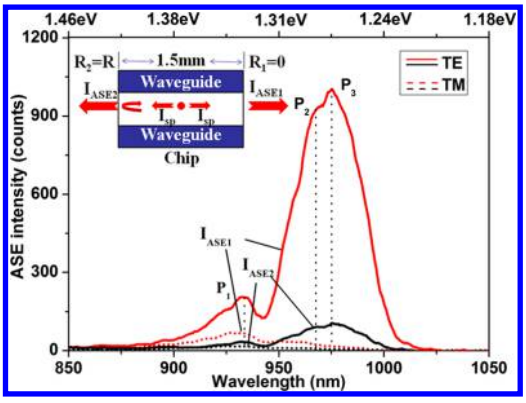

Figure 3. Measurement of ASE spectra from both facets of the in-plane sample with the InGaAs-based well−island composite structure. The carrier density due to optical injection is 9.6 × 10^{17} cm^{-3}.

It is clearly observed from Figure 3 that the ASE spectrum is apparently broadened but nonuniform. Three peaks P_1−P_3 are clearly observed from the ASE curves in TE mode, which include a main peak, P_3 (975 nm), and two minor peaks, P_1 (934 nm) and P_2 (965 nm).

It is noticed that since indium-rich islands consist of indium atoms or InAs compounds rather than InGaAs materials, these islands do not contribute to the ASE spectrum ranging from 850 to 1050 nm because the unstrained InAs compound has a band gap of 0.35 eV, which corresponds to the emission wavelength of 3.5 μm, and the compressively strained InAs/GaAs quantum dots produce an emission with a peak wavelength of 1.3 μm due to a large lattice mismatch.[26,27] The island's role leads to reduction of the indium content in the normal $In_xGa_{1-x}As$ material and forms many discrete indium content-reduced InGaAs regions. These regions, together with the normal InGaAs parts, produce the special ASE spectra shown in Figure 3.

The multipeak structure is the most typical feature of the indium-rich island formation. In terms of the model-solid theory,[25] the x-value in $In_xGa_{1-x}As$ can be obtained from the band gap calculation by the peak positions in the ASE spectrum. The result shows that these peaks corresponds to the emissions from the $In_xGa_{1-x}As$ materials with x = 0.17, x = 0.15, and x = 0.12, respectively. Since $In_{0.17}Ga_{0.83}As$ is the basic quantum well material from the original design, $In_{0.15}Ga_{0.85}As$ and $In_{0.12}Ga_{0.88}As$ are obviously two derivatives with reduced contents and distribute in the structure due to the indium-rich island effect. Hence, a multiple-peak configuration in the ASE spectrum will be a remarkable feature of the indium-rich island effect taking place for the InGaAs-based quantum well structure. The results of the multiple peaks in Figure 3 indicate that indium-deficient regions due to the indium-rich islands in the InGaAs well layer can be roughly classified into two parts, which have different indium contents of x = 0.12 and x = 0.15 from $In_{0.17}Ga_{0.83}As$. These two InGaAs regions, along with the primary $In_{0.17}Ga_{0.83}As$ make a major contribution to the ASE spectra in Figure 3. Certainly, the full ASE spectra also involve the emissions from more indium-deficient InGaAs regions, which have various indium contents and correspond to different sizes of indium-rich islands shown in Figure 2b.

The optical gain was obtained based on the ASE spectra measured from both facets of the in-plane sample, which is described in Figure 3. In this approach, the model gain, G, of the structure can be obtained by the following approach.[28]

$$G = \frac{1}{L}\ln\frac{(1-R)I_{ASE1} - I_{ASE2}}{R \times I_{ASE2}} \quad (1)$$

where I_{ASE1} and I_{ASE2} denote the ASE intensities measured at the end coated by T = 99.99% and the other uncoated end, respectively, of the sample, which are illustrated in Figure 3. R is the reflectivity of the uncoated facet and determined by the material indices. It is R = 30% here for the given sample. L is the single-pass distance, through which light propagates and is amplified within the sample. The optical gain spectra with different carrier densities of N = 9 × 10^{17}, 9.2 × 10^{17}, 9.4 × 10^{17}, and 9.6 × 10^{17} cm^{-3} due to optical injections are obtained and shown in Figure 4, where the internal loss coefficient α is about 3 cm^{-1} on average, indicated by the shadow area. In order to analyze optical power variation with wavelengths in the following section, the threshold gain, G_{th}, is also calculated below:

$$G_{th} = \alpha + \frac{1}{L}\ln\frac{1}{r_1 r_2} \quad (2)$$

where r_1 and r_2 are reflectivity of the cavity mirrors and assumed to be r_1 = 0.999 and r_2 = 0.9 for lasing here, so a threshold gain can be calculated by G_{th} = 3.77 cm^{-1}.

The results in Figure 4 reveal two very valuable characteristics. (1) The optical gain spectrum exhibits a very uniform distribution with the spectral flatness of 3.7 cm^{-1} in 906−996 nm or 1.07 cm^{-1} in 906−940 nm and 0.8 cm^{-1} in 958−992 nm for the TE mode under a certain injection power, even if the ASE spectrum shown in Figure 4 is nonuniform. This should

DOI: 10.1021/acsphotonics.8b01048
ACS Photonics 2018, 5, 4896−4902

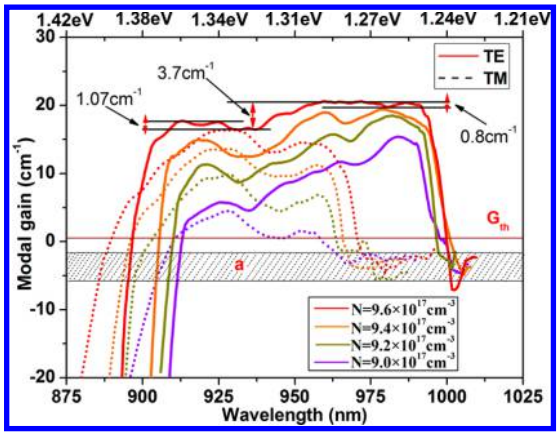

Figure 4. Gain spectra in TE and TM polarizations with various carrier densities of 9×10^{17}, 9.2×10^{17}, 9.4×10^{17}, and 9.6×10^{17} cm^{-3} from optical injections.

be attributed to the gain superposition from a large amount of indium-deficient InGaAs regions, which have various indium contents caused by the different sizes of indium-rich islands in the InGaAs layer and can be regarded as a sort of equivalent multiple well/dot structure to produce many different gain spectra and their superposition similar to the simulation described in Figure 1d. Thus, such a special structure enables the InGaAs-based tunable lasers to obtain more uniform spectral power over the full spectral tuning range. (2) The superwide flat-top gain distributions are obtained to be RSW ≥ 6 from the TE mode, compared with the standard gain bandwidth in Figure 1a obtained from a classic single InGaAs quantum well. This enables the spectral tuning range of the InGaAs-based lasers to be greatly enhanced, in comparison to the current level of RSW = 3.8.[20]

The energy bands and wave functions associated with the first conduction sub-band (C_1) and the first valence sub-bands of heavy holes (HH_1) and light holes (LH_1) of this special structure are initially analyzed in Figure 5. A relatively simple

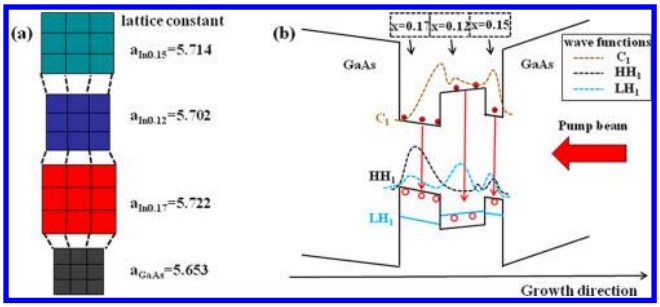

Figure 5. (a) Lattice mismatching of GaAs, $In_{0.17}Ga_{0.83}As$, $In_{0.15}Ga_{0.85}As$, and $In_{0.12}Ga_{0.88}As$ quantum-confined layers. (b) Energy bands and wave functions of the InGaAs/GaAs well−island composite quantum-confined structure.

model to consider the indium-rich island effect in the material growth direction is used for a fundamental insight, as the laterally random distribution of different sizes of indium-rich islands in the InGaAs layer will lead to more complicated mixing strain states and energy bands, which need more comprehensive investigation and is not the focus of this paper. In the model of Figure 5a, the $In_{0.12}Ga_{0.88}As$ layer locates between the $In_{0.17}Ga_{0.83}As$ and $In_{0.15}Ga_{0.85}As$ layers along the growth direction. This is because the indium-rich islands generally begin to occur and relax the accumulated high strain in the $In_{0.17}Ga_{0.83}As$ material after the $In_{0.17}Ga_{0.83}As$ is grown to exceed a few monolayers on GaAs.[24] With the continuous material growth and the strain relief due to the indium atom migration, the indium-rich island effect is attenuated so that more indium content is eventually preserved in the $In_xGa_{1-x}As$ layer near the surface.

Since the lattice constants of GaAs, $In_{0.17}Ga_{0.83}As$, $In_{0.12}Ga_{0.88}As$, and $In_{0.15}Ga_{0.85}As$ are 5.65325, 5.72215, 5.7019, and 5.71405 Å, respectively, the asymmetric compressive strain occurs in both $In_{0.17}Ga_{0.83}As$ and $In_{0.15}Ga_{0.85}As$ layers so that the HH_1 sub-band is higher than the LH_1 sub-band in these two materials, where the compressive strain in $In_{0.15}Ga_{0.85}As$ would be slightly less than that in $In_{0.17}Ga_{0.83}As$, as illustrated in Figure 5a. Meanwhile, the asymmetric tensile strain occurs in the $In_{0.12}Ga_{0.88}As$ layer so that the HH_1 sub-band becomes lower than the LH_1 sub-band in the structure.[29] The overall energy band structure is illustrated in Figure 5b, in which the first conduction sub-band (C_1) and the first valence sub-bands of heavy holes (HH_1) and light holes (LH_1) are of steps with different widths due to the asymmetric strains and the indium-rich island effect in the materials. In fact, similar mixing strain states would happen in the in-plane directions of the structure as well. This illustrates that a complicated mixing strain state exists in the InGaAs/GaAs well−island composite quantum-confined structure, and it will lead to very different optical gain characteristics.[30]

SPECTRAL POWER CHARACTERISTICS

The superwide and uniform gain distribution from the InGaAs-based well−island composite quantum-confined structure makes it possible to greatly enhance performance of the InGaAs-based tunable lasers in both extending spectral tuning range and realizing more uniform spectral power over all tunable wavelengths, especially at both ends of the spectral tuning range. This is based on the following analysis.

The relation between the material gain, g, and the current density can be expressed as[31]

$$g = \frac{A\eta_i\tau_{sp}}{ed}(J - J_{tr}) \tag{3}$$

$$J_{th} = J_{tr} + \frac{ed}{\Gamma\eta_i\tau_{sp}A}\left[a + \frac{1}{2L}\ln\left(\frac{1}{r_1r_2}\right)\right] \tag{4}$$

where A is a constant. τ_{sp} denotes radiative recombination lifetime. η_i represents the internal quantum efficiency. J is the current density, and J_{th} denotes the threshold current density. d is the thickness of the active layer, and e is the elementary charge. J_{tr} represents transparency current density. Γ is the confinement factor.

According to eqs 3 and 4, the current density above the threshold can be written as

$$J - J_{th} \propto \left[\Gamma g - a - \frac{1}{2L}\ln\left(\frac{1}{r_1r_2}\right)\right] \tag{5}$$

As the lasing power is $P_{out} \propto (J - J_{th})$, the power can be expressed as

DOI: 10.1021/acsphotonics.8b01048
ACS Photonics 2018, 5, 4896−4902

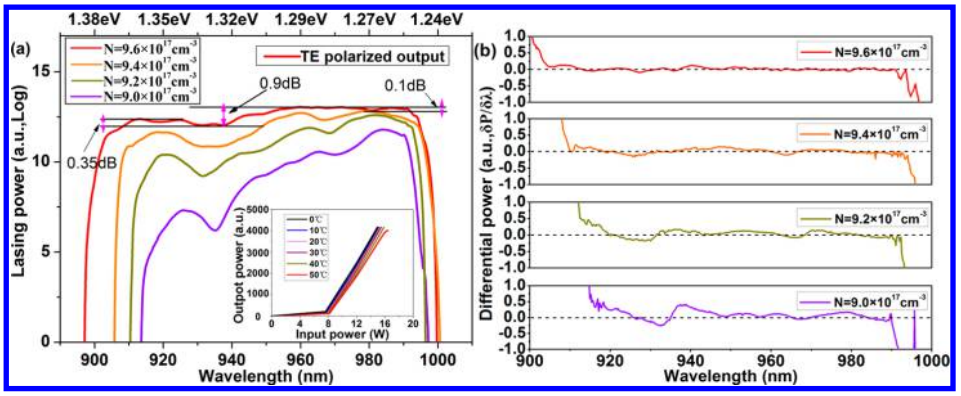

Figure 6. (a) Spectral power as a function of wavelength with various carrier densities. (b) Differentials of power spectra with various carrier densities.

$$P_{out} \propto \left[G - \frac{1}{2L} \ln\left(\frac{1}{r_1 r_2}\right) \right] \quad (6)$$

Thus, the relative power distribution can be characterized by substituting the gain data into eq 6. As an example, the power as a function of wavelength is calculated by substituting the gain data given in Figure 4 into eq 6, and the result is shown in Figure 6a. Obviously, the power is proportional to the gain. Thus, the wavelength tuning range of the output power can be up to RSW ≥ 6 (906−996 nm) with the spectral flatness of 0.9 dB, 958−992 nm with a flatness of 0.1 dB, and 906−940 nm with a flatness of 0.35 dB under a carrier density of 9.6×10^{17} cm^{-3}. From the trend of spectral power variation with carrier densities, it can be predicted that the power will become further uniform over the total spectral tuning range, as the carrier density is increased. Figure 6b shows the differential power as a function of wavelength with different carrier densities. Clearly, the differential power with a smaller deviation to zero indicates more uniform output power over the full spectral tuning range.

Experimentally, the lasing with various temperatures was obtained using the edge-emitting sample with the $In_{0.17}Ga_{0.83}As/GaAs/GaAsP_{0.08}$ well−island composite structure described in section one, where both facets of the sample were uncoated. The measured result is shown as the inset of Figure 6a.

CONCLUSIONS

In this paper, we have reported a special InGaAs-based well−island composite quantum-confined structure, which achieves the best result to date in realizing both very uniform and superwide gain and power spectra. So the performance of the InGaAs-based tunable semiconductor lasers may be tremendously enhanced. This special structure is associated with the indium-rich island effect generated in the material growth, in which the mixing strain states containing both compressive and tensile strains occur and affect the optical gain characteristics. The investigation on this special structure and its unusual optical characteristics has been conducted only initially here. It is believed that a more comprehensive investigation on it will achieve semiconductor lasers with better performances in the near future.

AUTHOR INFORMATION

Corresponding Author

*E-mail: jwu2@buaa.edu.cn.

ORCID

Jian Wu: 0000-0002-0635-3857

Notes

The authors declare no competing financial interest.

ACKNOWLEDGMENTS

The authors gratefully acknowledge the financial support of the National Natural Science Foundation of China (Grant Nos. 61376067, 61474118) for this work.

REFERENCES

(1) Ren, Y.; Hovenier, J. N.; Higgins, R.; Gao, J. R.; Klapwijk, T. M.; Shi, S. C.; Klein, B.; Kao, T. Y.; Hu, Q.; Reno, J. L. High-resolution heterodyne spectroscopy using a tunable quantum cascade laser around 3.5 THz. *Appl. Phys. Lett.* **2011**, *98*, 231109.

(2) Mateus, C. F. R.; Huang, M. C. Y.; Li, P.; Cunningham, B. T.; Chang-Hasnain, C. J. Compact label-free biosensor using VCSEL-based measurement system. *IEEE Photonics Technol. Lett.* **2004**, *16*, 1712−1714.

(3) Totschnig, G.; Lackner, M.; Shau, R.; Ortsiefer, M.; Rosskopf, J.; Amann, M. C.; Winter, F. 1.8 μm vertical-cavity surface-emitting laser absorption measurements of HCl, H2O and CH4. *Meas. Sci. Technol.* **2003**, *14*, 472−478.

(4) Mateus, C. F. R.; Huang, M. C. Y.; Chang-Hasnain, C. J.; Foley, J. E.; Beatty, R.; Li, P.; Cunningham, B. T. Ultra-sensitive immunoassay using VCSEL detection system. *Electron. Lett.* **2004**, *40*, 649−651.

(5) Klinkhammer, S.; Liu, X.; Huska, K.; Shen, Y. X.; Vanderheiden, S.; Valouch, S.; Vannahme, C.; Bräse, S.; Mappes, T.; Lemmer, U. Continuously tunable solution-processed organic semiconductor DFB lasers pumped by laser diode. *Opt. Express* **2012**, *20*, 6357−6364.

(6) Harvey, K. C.; Myatt, C. J. External-cavity diode laser using a grazing-incidence diffraction grating. *Opt. Lett.* **1991**, *12*, 910−912.

(7) Jechow, A.; Raab, V.; Menzel, R.; Cenkier, M.; Stry, S.; Sacher, J. 1 W tunable near diffraction limited light from a broad area laser diode in an external cavity with a line width of 1.7 MHz. *Opt. Commun.* **2007**, *277*, 161−165.

(8) Schwarzbäck, T.; Kahle, H.; Eichfelder, M.; Roßbach, R.; Jetter, M.; Michler, P. Wavelength tunable ultraviolet laser emission via intra-cavity frequency doubling of an AlGaInP vertical external-cavity surface-emitting laser down to 328 nm. *Appl. Phys. Lett.* **2011**, *99*, 261101.

(9) Fan, L.; Fallahi, M.; Hader, J.; Murray, J. T.; Bedford, R.; Kaneda, Y.; Zakharian, A. R.; Hader, J.; Moloney, J. V.; Stolz, W.; Koch, S. W. Tunable high-power high-brightness linearly polarized vertical-external-cavity surface-emitting lasers. *Appl. Phys. Lett.* **2006**, *88*, 021105.

DOI: 10.1021/acsphotonics.8b01048
ACS Photonics 2018, 5, 4896−4902

(10) Martyshkin, D.; Kesterson, T.; Fedorov, V. V.; Mirov, S. Mid-IR CW Cr:ZnS laser tunable with acousto-optical filter. *Proc. SPIE* **2017**, *10082*, 100820G−1.
(11) Huang, M. C. Y.; Cheng, K. B.; Zhou, Y. Monolithic Integrated Piezoelectric MEMS-Tunable VCSEL. *IEEE J. Sel. Top. Quantum Electron.* **2007**, *13*, 374−380.
(12) Jung, S. Y.; Jiang, A.; Jiang, Y. F.; Vijayraghavan, K.; Wang, X. J.; Troccoli, M.; Belkin, M. A. Broadly tunable monolithic room-temperature terahertz quantum cascade laser sources. *Nat. Commun.* **2014**, *5*, 4267.
(13) Vijayraghavan, K.; Jiang, Y. F.; Jang, M.; Jiang, A.; Choutagunta, K.; Vizbaras, A.; Demmerle, F.; Boehm, G.; Amann, M. C.; Belkin, M. A. Broadly tunable terahertz generation in mid-infrared quantum cascade lasers. *Nat. Commun.* **2013**, *4*, 2021.
(14) Gotoda, M.; Takabayashi, M.; Horiguchi, Y.; Matsumoto, K.; Ishimura, E. Dual-Output Tunable Laser Diode Array for Optical Transmission and Coherent Detection. *IEEE J. Sel. Top. Quantum Electron.* **2017**, *23*, 6000406.
(15) Kameda, T.; Mori, H.; Onuki, S.; Kikugawa, T.; Takahashi, Y.; Tsuchiya, F.; Nagai, H. A. DBR Laser Employing Passive-Section Heaters, with 10.8nm Tuning Range and 1.6 MHz Linewidth. *IEEE Photonics Technol. Lett.* **1993**, *5*, 608−610.
(16) Jechow, A.; Raab, V.; Menzel, R.; Cenkier, M.; Stry, S.; Sacher, J. 1 W tunable near diffraction limited light from a broad area laser diode in an external cavity with a line width of 1.7 MHz. *Opt. Commun.* **2007**, *277*, 161−165.
(17) Fan, L.; Fallahi, M.; Zakharian, A. R.; Hader, J.; Moloney, J. V.; Bedford, R.; Murray, J. T.; Stolz, W.; Koch, S. W. Extended Tunability in a Two-Chip VECSEL. *IEEE Photonics Technol. Lett.* **2007**, *19*, 544−546.
(18) Zhou, W.; Wu, D.; Mcclintock, R.; Slivken, S.; Razeghi, M. High performance monolithic, broadly tunable mid-infrared quantum cascade lasers. *Optica* **2017**, *4*, 1228−1231.
(19) Khan, M. Z. M.; Alhashim, H. H.; Ng, T. K.; Ooi, B. S. High-power and high-efficiency 1.3-μm superluminescent diode with flat-top and ultrawide emission bandwidth. *IEEE Photonics J.* **2015**, *7*, 1−8.
(20) Haffouz, S.; Barrios, P. J.; Normandin, R.; Poitras, D.; Lu, Z. Ultrawide-bandwidth, superluminescent light-emitting diodes using InAs quantum dots of tuned height. *Opt. Lett.* **2012**, *37*, 1103−1105.
(21) Zhou, K. J.; Jiang, Q.; Zhang, Z. Y.; Chen, S. M.; Liu, H. Y.; Lu, Z. H.; Kennedy, K.; Matcher, S. J.; Hogg, R. A. Quantum dot selective area intermixing for broadband light sources. *Opt. Express* **2012**, *20*, 26950−26957.
(22) Jasik, A.; Wnuk, A.; Wojcik-Jedlinska, A.; Jakiela, R.; Muszalski, J.; Strupinski, W.; Bugajski, M. The influence of the growth temperature and interruption time on the crystal quality of InGaAs/GaAs QW structures grown by MBE and MOCVD methods. *J. Cryst. Growth* **2008**, *310*, 2785−2792.
(23) Yu, H. P.; Roberts, C.; Murray, R. Influence of indium segregation on the emission from InGaAs/GaAs quantum wells. *Appl. Phys. Lett.* **1995**, *66*, 2253−2255.
(24) Schlenker, D.; Miyamoto, T.; Chen, Z.; Koyama, F.; Iga, K. Growth of highly strained GaInAs/GaAs quantum wells for 1.2 μm wavelength lasers. *J. Cryst. Growth* **2000**, *209*, 27−36.
(25) Van de Walle, C. G. Band lineups and deformation potentials in the model-solid theory. *Phys. Rev. B: Condens. Matter Mater. Phys.* **1989**, *39*, 1871−1883.
(26) Chen, S. M.; Tang, M. C.; Jiang, Q.; Wu, J.; Dorogan, V. G.; Benamara, M.; Mazur, Y. I.; Salamo, G. J.; Smowton, P.; Seeds, A.; Liu, H. Y. InAs/GaAs Quantum-Dot Superluminescent Light-Emitting Diode Monolithically Grown on a Si Substrate. *ACS Photonics* **2014**, *1*, 638−642.
(27) Jung, D.; Zhang, Z. Y.; Norman, J.; Herrick, R.; Kennedy, M. J.; Patel, P.; Turnlund, K.; Jan, C.; Wan, Y. T.; Gossard, A. C.; Bowers, J. E. Highly Reliable Low-Threshold InAs Quantum Dot Lasers on On-Axis (001) Si with 87% Injection Efficiency. *ACS Photonics* **2018**, *5*, 1094−1100.
(28) Coldren, L. A. *Diode Lasers and Photonic Integrated Circuits*, 2th ed.; Wiley: Hoboken, 2012; pp 167−168.
(29) Zhou, W.; Shen, H.; Pamulapati, J.; Cooke, P.; Dutta, M. Heavy- and light-hole band crossing in a variable-strain quantum-well heterostructure. *Phys. Rev. B: Condens. Matter Mater. Phys.* **1995**, *51*, 5461−5464.
(30) Ma, M. L.; Wu, J.; Ning, Y. Q.; Zhou, F.; Yang, M.; Zhang, X.; Zhang, J.; Shang, G. Y. Measurement of gain characteristics of semiconductor lasers by amplified spontaneous emissions from dual facets. *Opt. Express* **2013**, *21*, 10335−10341.
(31) Basu, P. K.; Mukhopadhyay, B.; Basu, R. *Semiconductor Laser Theory*; Taylor& Francis Group, LLC, 2016; pp 234−235.

DOI: 10.1021/acsphotonics.8b01048
ACS Photonics 2018, 5, 4896−4902